

Composable Score-based Graph Diffusion Model for Multi-Conditional Molecular Generation

Anjie Qiao
Zhen Wang*
Chuan Chen

1. Sun Yat-sen University

QIAOANJ@MAIL2.SYSU.EDU.CN
WANGZH665@MAIL.SYSU.EDU.CN
CHENCHUAN@MAIL.SYSU.EDU.CN

DeFu Lian
Enhong Chen

2. University of Science and Technology of China

LIANDEFU@USTC.EDU.CN
CHENEH@MAIL.USTC.EDU.CN

Abstract

Controllable molecular graph generation is essential for material and drug discovery, where generated molecules must satisfy diverse property constraints. While recent advances in graph diffusion models have improved generation quality, their effectiveness in multi-conditional settings remains limited due to reliance on joint conditioning or continuous relaxations that compromise fidelity. To address these limitations, we propose Composable Score-based Graph Diffusion model (CSGD), the first model that extends score matching to discrete graphs via concrete scores, enabling flexible and principled manipulation of conditional guidance. Building on this foundation, we introduce two score-based techniques: Composable Guidance (CoG), which allows fine-grained control over arbitrary subsets of conditions during sampling, and Probability Calibration (PC), which adjusts estimated transition probabilities to mitigate train–test mismatches. Empirical results on four molecular datasets show that CSGD achieves state-of-the-art performance, with a 15.3% average improvement in controllability over prior methods, while maintaining high validity and distributional fidelity. Our findings highlight the practical advantages of score-based modeling for discrete graph generation and its capacity for flexible, multi-property molecular design.

1. Introduction

Molecular graph generation is pivotal for material and drug discovery, enabling efficient exploration of vast chemical spaces [8, 42]. For real-world applications, a key challenge lies in controlling the generation process so that molecules satisfy multiple desired properties [13]. For instance, one may wish to generate a set of candidate molecules that simultaneously meet specific ranges of synthetic scores and permeability to target gases.

Recent advances in graph diffusion models [28, 41, 45] have significantly improved molecular generation quality. However, their ability in multi-conditional generation remains to be improved. Early approaches [4, 27] collapse all properties into a single joint condition (Figure 1A), which obscures the influence of individual properties and hinders fine-grained control. GraphDiT [28] mitigates this issue by designing separate encoders for categorical and numerical conditions (Figure 1C), yet still treats the combination of encodings as a monolithic condition. This rigid design prevents dynamic inclusion or exclusion of conditions.

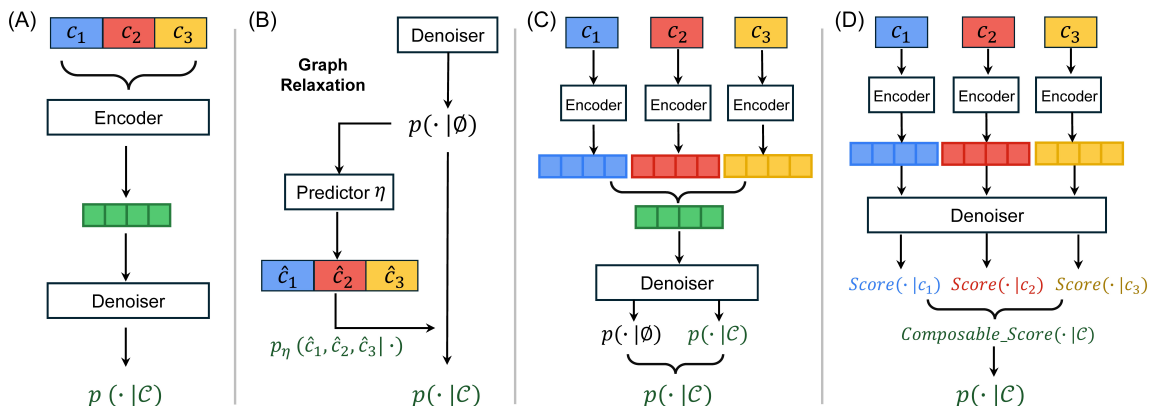


Figure 1: Comparison of multi-conditional guidance in discrete graph diffusion: (A) vanilla conditional generation; (B) predictor guidance in DiGress; (C) predictor-free guidance in GraphDiT; (D) our composable score-based guidance. For clarity, the sampling process and notation are simplified.

Therefore, a natural question arises: Is it viable to flexibly compose the guidance of each property considered for molecular graph generation? In analogy to classifier guidance in continuous domain [7], DiGress [41] proposes predictor-guidance by combining the gradients from multiple property predictors (Figure 1B). However, this requires relaxing discrete graphs into continuous variables, potentially degrading generation fidelity. Meanwhile, existing discrete graph diffusion models [38, 41, 45] typically adopt the mean prediction [2, 5], where the denoiser predicts the clean sample’s distribution based on the current noisy and the given condition, rather than the score of the current marginal distribution. This design makes score-based compositional guidance inapplicable [29], and directly composing the estimated distributions of each considered condition lacks theoretical interpretation.

To overcome these limitations, we propose **Composable Score-based Graph Diffusion** model (CSGD), a novel model for flexible multi-conditional molecular generation. Built upon the recently proposed concrete score [30], we introduce concrete score-based diffusion model for discrete graphs, extending score matching to this domain. This design unlocks advanced score manipulation techniques. Specifically, we introduce *Composable Guidance*, a novel mechanism that leverages the compositional nature of the score for multi-conditional generation (Figure 1D). Then, we explore *Probability Calibration*, manipulating conditional concrete scores to better shape the estimated transition probabilities within the generation process. With these techniques, CSGD achieves flexible, property-aware sampling and significantly improves both validity and controllability. In summary, our contributions are as follows:

- To the best of our knowledge, we introduce the first concrete score-based graph diffusion model, which extends score matching to discrete graph generation and enabling advanced score-manipulation techniques that were previously inapplicable.

- We propose *Composable Guidance* and *Probability Calibration* for multi-conditional molecular generation, which manipulate per-property scores to steer generation toward satisfying desired properties, thereby improving the validity and controllability of the generated molecules.
- We compare CSGD with various multi-conditional molecular generation methods (Figure 1A-C) on four public datasets. CSGD achieves state-of-the-art performance, with an average 15.3% improvement in controllability, highlighting the effectiveness of score-based modeling and composable guidance.

2. Related Works

Graph Diffusion Models. Diffusion models [2, 17, 39] have been widely applied to graph generation. Early approaches such as EDP-GNN [32] and GDSS [20] treated graphs as continuous variables, typically using a Gaussian reference distribution, similar to that in image generation. Because graphs are inherently discrete, subsequent work [28, 38, 41] modeled graphs in discrete state spaces to better capture their structural properties. Among them, DiGress [41] demonstrated strong performance on various graph generation benchmarks and thus has been widely adopted in practice. However, these models generally operate in a discrete time setting, which limits the flexibility of sampling [45]. To address this, recent methods such as DISCO [45] and COMETH [38] first introduce discrete-state, continuous-time diffusion models for graph generation. In this work, our proposed CSGD also operates with continuous time and discrete state, while distinct from previous methods by introducing the concrete score [30], thereby unlocking score-manipulation techniques for guided sampling that would otherwise be unavailable for the existing mean prediction-based graph diffusion models.

Guidance for diffusion model. Recent studies [1, 18, 29] have shown that sampling guidance techniques, such as classifier guidance [7] and classifier-free guidance [16], are crucial for steering diffusion models toward samples that better respect satisfy condition(s). As classifier-free guidance has shown its superiority in many tasks, many recent works proposed improvements to it, including applying guidance only during the middle interval of sampling to improve inference speed and quality [26], guiding a high-quality model with a degraded, lower-quality model trained on the same task and data [22], a first-principles nonlinear correction [48], sliding window guidance [21], and independent condition guidance [36]. These techniques have proven effective in improving the sample quality and condition obedience. Building on our introduction of concrete score, we further propose two score-manipulation techniques to improve the validity and controllability of discrete graph generation.

3. Methodology

In this section, we present CSGD, which tailors SEDD [30] to the domain of multi-conditional molecular generation (see Section 3.1). Leveraging the composable nature of the scores, CSGD enables more flexible and controllable sampling strategies for generation tasks conditioning on multiple properties (see Section 3.2). In analogy to recently proposed tricks for scores in the continuous domain, we propose Probability Calibration (PC) mechanism for CSGD to improve the validity and controllability of the generated molecular graphs (see Section 3.3).

Notations and Problem Definition. We model graphs in a discrete space, where nodes and edges take categorical attributes, denoted by $\mathcal{X} = \{1, \dots, a\}$ and $\mathcal{E} = \{1, \dots, b\}$, respectively. A graph

is represented as $G = (\mathbf{X}, \mathbf{E})$, where $\mathbf{X} = (x^i)_{i=1}^n \in \mathcal{X}^n$ specifies each node’s type (i.e., atom type) and $\mathbf{E} = (e^{ij})_{i,j=1}^n \in \mathcal{E}^{n \times n}$ specifies each edge’s type (i.e., bond type or the indicator of no connection). Here, n denotes the number of nodes. Let $\mathcal{C} = \{c_1, c_2, \dots, c_M\}$ denote a set of M specified conditions, where c_i may be numerical or categorical. The multi-conditional molecular generation is to model: $p(G|\mathcal{C}) = p(G|c_1, \dots, c_M) \propto p(G)p(c_1, \dots, c_M|G)$, where molecular graph G can be evaluated along two dimensions: (1) Distribution Learning $p(G)$: measuring the fidelity to the underlying unconditional distribution; (2) Controllability $p(c_1, \dots, c_M|G)$: measuring consistency between generated molecular graph and the specified conditions. Moreover, there are often practical scenarios in which we need to sample G with only a subset of properties specified. A flexible solution is demanded that can handle an arbitrary subset of properties based on one common model.

3.1. Score-based Graph Diffusion Model

For brevity, we present our diffusion model in an unconditional setting to focus on the use of the concrete score [31]. This unconditional formulation can be readily adapted to our target multi-conditional generation problem simply by feeding the encoded condition(s) into the denoiser.

Diffusion Process. Following prior graph diffusion models [45], we diffuse each node and each edge independently following a continuous-time Markov process, which can be described by linear ODEs [30]:

$$\frac{dp_t^X}{dt} = Q_t^X p_t^X, \quad \frac{dp_t^E}{dt} = Q_t^E p_t^E, \quad (1)$$

where $\forall t \in \mathbb{R}_+$, $p_t^X \in \mathbb{R}^a$, $p_t^E \in \mathbb{R}^b$ denote the marginal discrete probability distributions, with boundary conditions $p_0 \approx p_{\text{data}}$ and $p_{t \rightarrow \infty} \approx p_{\text{base}}$. With a scalar noise schedule $\sigma(t)$ [17], the time-dependent transition matrices are defined as $Q_t^X = \sigma(t)Q^X$ and $Q_t^E = \sigma(t)Q^E$, where $Q^X \in \mathbb{R}^{a \times a}$ and $Q^E \in \mathbb{R}^{b \times b}$ are the transition matrices for nodes and edges, respectively. Due to this independence, the likelihood of a graph G_t at timestep t is factorized as $p_t(G_t) = \prod_{i=1}^n p_t^X(x_t^i) \prod_{i,j=1}^n p_t^E(e_t^{ij})$. We adopt two common choices for the transition matrix Q^X (resp. Q^E): *Absorb* [5], which introduces a dedicated absorbing (MASK) state, and *Uniform* [2], which assigns the same transition probabilities to all other states.

Then, the element-wise forward transition admits a closed form. Conditioned on the state at $t = 0$, the probability is given by the cumulative transition matrix:

$$\begin{aligned} p_{t|0}^X(\cdot|x_0^i = x) &= x\text{-th column of } \exp(\bar{\sigma}(t)Q^X), \\ p_{t|0}^E(\cdot|e_0^{ij} = e) &= e\text{-th column of } \exp(\bar{\sigma}(t)Q^E), \end{aligned} \quad (2)$$

where $\bar{\sigma}(t) = \int_0^t \sigma(s) ds$ is the cumulative noise coefficient. Thus, the likelihood of the entire graph G_t conditioned on the observation G_0 is given by $p_{t|0}(G_t|G_0) = \prod_{i=1}^n p_{t|0}^X(x_t^i|x_0^i) \prod_{i,j=1}^n p_{t|0}^E(e_t^{ij}|e_0^{ij})$.

Reverse Process. The reverse process aims to reconstruct graphs obeying p_{data} from noisy ones sampled from p_{base} , which can be completed via simulating the reversal of Eq. (1), that is, $\frac{dp_{T-t}^X}{dt} = \bar{Q}_{T-t}^X p_{T-t}^X$ and $\frac{dp_{T-t}^E}{dt} = \bar{Q}_{T-t}^E p_{T-t}^E$ [23, 40]. Since the flux should be consistent, that is, $\bar{Q}_t^X(x', x)p_t^X(x) = Q_t^X(x, x')p_t^X(x')$, existing works [31] have proposed to estimate the ratio $\frac{p_t^X(x')}{p_t^X(x)}$, namely concrete

score, and use these scores to perform the reverse process. Edges can be treated analogously via $\frac{p_t^E(e')}{p_t^E(e)}$.

Due to the combinatorial nature of discrete graphs, a general transition matrix defining probabilities between all possible graph pairs is clearly intractable. Thanks to the independence design of our diffusion process, we restrict each transition to flip only a single position—either a node or an edge—at a time. Under this design, the concrete scores can be naturally parameterized using a neural network $s_\theta(\cdot, \cdot)$:

$$\begin{aligned} s_\theta^X(G_t, t)_{i, \tilde{x}_t^i} &\approx \frac{p_t^X(x_t^1 \dots \tilde{x}_t^i \dots x_t^n)}{p_t^X(x_t^1 \dots x_t^i \dots x_t^n)} \text{ for } 1 \leq i \leq n, \tilde{x}_t^i \neq x_t^i, \\ s_\theta^E(G_t, t)_{ij, \tilde{e}_t^{ij}} &\approx \frac{p_t^E(e_t^{11} \dots \tilde{e}_t^{ij} \dots e_t^{nn})}{p_t^E(e_t^{11} \dots e_t^{ij} \dots e_t^{nn})} \text{ for } 1 \leq i, j \leq n, \tilde{e}_t^{ij} \neq e_t^{ij}. \end{aligned} \quad (3)$$

Here, x_t^i (resp. e_t^{ij}) denotes the current node (resp. edge) state and \tilde{x}_t^i (resp. \tilde{e}_t^{ij}) are possible alternative states from the corresponding discrete space. Specifically, $s_\theta(\cdot, \cdot)$ is often a Graph Transformer that processes both node tokens and edge tokens, where the subscripts (i, \tilde{x}_t^i) mean to take its \tilde{x}_t^i -th output dimension at the i -th node token, with edges treated analogously.

Following SEDD, we borrow the derivation of Tweedie denoising [9] yet perform τ -leaping, with each token states x_s^i and e_s^{ij} at timestep $s = t - \Delta t$, $\Delta t \geq 0$ having their conditional probabilities as follows:

$$\begin{aligned} p_{s|t}^X(x_s^i | x_t^i; \theta) &= (\exp(-\sigma_t^{\Delta t} Q^X) s_\theta^X(G_t, t)_{x_s^i}) \exp(\sigma_t^{\Delta t} Q^X)(x_t^i, x_s^i), \\ p_{s|t}^E(e_s^{ij} | e_t^{ij}; \theta) &= (\exp(-\sigma_t^{\Delta t} Q^E) s_\theta^E(G_t, t)_{e_s^{ij}}) \exp(\sigma_t^{\Delta t} Q^E)(e_t^{ij}, e_s^{ij}), \end{aligned} \quad (4)$$

where $\sigma_t^{\Delta t} = \bar{\sigma}(t) - \bar{\sigma}(s)$. Specifically, we perform Euler step for each token independently based on Eq. (4) yet with τ -leaping. Essentially, the reverse step factorizes across tokens:

$$p_{s|t}(G_s | G_t; \theta) = \prod_{i=1}^n p_{s|t}^X(x_s^i | x_t^i; \theta) \prod_{i,j=1}^n p_{s|t}^E(e_s^{ij} | e_t^{ij}; \theta). \quad (5)$$

Optimization. The denoiser s_θ is trained to predict concrete scores by minimizing the *Diffusion Weighted Denoising Score Entropy* [30]:

$$\begin{aligned} \mathcal{L}_t^X(G_0, G_t, \theta) &= \sigma(t) \sum_{i=1}^n \sum_{\tilde{x}_t^i=1}^a (1 - \delta_{x_t^i}(\tilde{x}_t^i)) \left(s_\theta^X(G_t, t)_{i, \tilde{x}_t^i} - \frac{p_{t|0}(\tilde{x}_t^i | x_0^i)}{p_{t|0}(x_t^i | x_0^i)} \right) \log s_\theta^X(G_t, t)_{i, \tilde{x}_t^i}, \\ \mathcal{L}_t^E(G_0, G_t, \theta) &= \sigma(t) \sum_{i,j=1}^n \sum_{\tilde{e}_t^{ij}=1}^b (1 - \delta_{e_t^{ij}}(\tilde{e}_t^{ij})) \left(s_\theta^E(G_t, t)_{ij, \tilde{e}_t^{ij}} - \frac{p_{t|0}(\tilde{e}_t^{ij} | e_0^{ij})}{p_{t|0}(e_t^{ij} | e_0^{ij})} \right) \log s_\theta^E(G_t, t)_{ij, \tilde{e}_t^{ij}}. \end{aligned} \quad (6)$$

The Kronecker delta $\delta_{x_t^i}(\tilde{x}_t^i)$ and $\delta_{e_t^{ij}}(\tilde{e}_t^{ij})$ ensures that the current state is excluded from the summation. The final loss combines node and edge terms with weight λ as $\mathcal{L}_t(G_0, G_t, \theta) = \mathcal{L}_t^X(G_0, G_t, \theta) + \lambda \mathcal{L}_t^E(G_0, G_t, \theta)$. The score entropy loss is well-suited for recovering the ground-truth concrete scores [30]. We optimize it using the Adam [24] optimizer, with gradient clipping and a learning rate warmup [15] to stabilize training.

Analysis. Suppose we discretize the reversal of Eq. 1 by timesteps $0 = t_0 < t_1 < \dots < t_{T-1} < t_T = 1$ and simulate the process to sample G_0 , the corresponding estimated distribution is $p(G; \theta) = \sum_{G_{t_1}, \dots, G_{t_T}} \prod_{k=1}^T p_{t_{k-1}|t_k}(G_{t_{k-1}}|G_{t_k}; \theta) p_{\text{base}}(G_{t_T})$. Since isomorphic molecular graphs are treated equally, the permutation-invariant $p(G; \theta)$ is preferred.

Proposition 1 *The estimated distribution $p(G; \theta)$ is permutation-invariant.*

Proof According to the theoretical results of GeoDiff [44], we just need to show that (1) the base distribution p_{base} is permutation-invariant and (2) the transitions $p_{t_{k-1}|t_k}(G_{t_{k-1}}|G_{t_k}; \theta)$ are permutation-equivariant.

At first, no matter whether to choose Absorb or Uniform, p_{base} is factorized over i.i.d. node and edge distributions.

Our denoiser is implemented as a Graph Transformer [28], which is permutation-equivariant: any permutation π_n of the input tokens induces the corresponding permutation π_n on its output tokens. Hence, the transitions $p_{t_{k-1}|t_k}(G_{t_{k-1}}|G_{t_k}; \theta)$ is permutation-equivariant according to Eq. 4.

As these two conditions are satisfied, we have that $p(\pi_n.G; \theta) = p(G; \theta)$. \blacksquare

3.2. Multi-conditional Molecular Generation via Concrete Scores

As discussed at the beginning of this Section, we focus on multi-conditional molecular generation, where the observed dataset $\mathcal{D} = \{(G, \mathcal{C})_l\}_{l=1}^N$ is an unbiased sample drawn from the underlying joint distribution. Our goal is to estimate the conditional distribution $p(G|\mathcal{C})$ so that we can sample molecular graphs that are valid and respect the specified properties \mathcal{C} . We will elaborate on how to achieve this goal with our score-based graph diffusion model and further to enable the flexible specification of an arbitrary subset of the M properties.

Classifier-free guidance (CFG). We first employ the same classifier-free guidance (CFG) as GraphDiT (see Figure 1C). During training and inference, all M properties are encoded and combined into a joint condition embedding, which is fed into the backbone of the denoiser to produce multi-conditional score. Then, both this conditional score and the unconditional one are merged to guide generation. Specifically, given a guidance scale w , the CFG score is:

$$s_{\theta}^{\text{CFG}}(G_t, \mathcal{C}, t) = s_{\theta}(G_t, \emptyset, t) + w (s_{\theta}(G_t, \mathcal{C}, t) - s_{\theta}(G_t, \emptyset, t)). \quad (7)$$

As can be seen, CFG treats all properties as a whole \mathcal{C} , producing a single monolithic score $s_{\theta}(G_t, \mathcal{C}, t)$ and limiting fine-grained control over individual properties c_m .

Composable Guidance (CoG). We illustrate one simulation step of CSGD with CoG in Figure 2, where the goal is to flexibly generate molecules conditioned on arbitrary subsets of all the M properties. To this end, we rely on the decomposition of multi-conditional probability:

$$p(G|c_1, \dots, c_M) \propto p(G)p(c_1, \dots, c_M|G) = p(G) \prod_{m=1}^M p(c_m|G) = p(G) \prod_{m=1}^M \frac{p(G|c_m)p(c_m)}{p(G)}, \quad (8)$$

where we assume conditional independence of the properties given G , and we substitute each conditional likelihood $p(c_m|G)$ by: $p(c_m|G) = \frac{p(G|c_m)p(c_m)}{p(G)}$. Following prior work on compositional

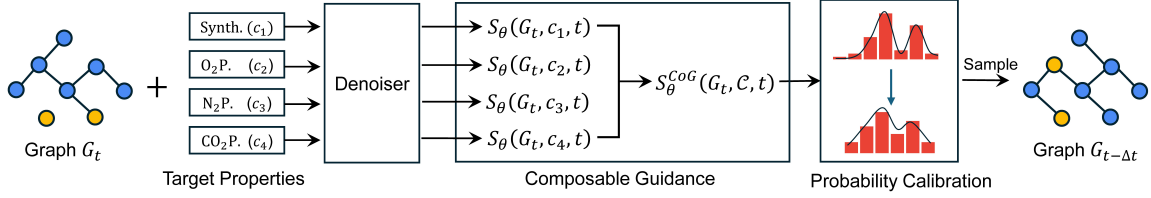


Figure 2: An overview of CSGD with Composable Guidance (CoG) to enable flexible control (P.: Gas Permeability; Synth.: Synthesizability).

Algorithm 1: Training a Score-based Graph Diffusion Model for CoG.

Input: Denoiser s_θ , dataset $\mathcal{D} = \{(G, \mathcal{C})_l\}_{l=1}^N$, transition matrices Q^X, Q^E , noise schedule $\bar{\sigma}$, loss weight λ .

Output: Trained denoiser s_θ .

while until convergence do

Get a pair (G, \mathcal{C}) from \mathcal{D} and let $G_0 \leftarrow G$;
 Sample timestep $t \sim \mathcal{U}(0, 1)$ and property $c_m \in \mathcal{C}$;
 Construct noisy graph G_t : $x_t^i \sim p_{t|0}^X(\cdot|x_0^i)$, $e_t^{ij} \sim p_{t|0}^E(\cdot|e_0^{ij})$ based on Eq. 2;
 Randomly set $c_m \leftarrow \emptyset$ with a probability to enable unconditional training;
 Predict concrete scores: $(s_\theta^X, s_\theta^E) \leftarrow s_\theta(G_t, c_m, t)$;
 Compute loss $\mathcal{L}_t(G_0, G_t, \theta) = \mathcal{L}_t^X(G_0, G_t, \theta) + \lambda \mathcal{L}_t^E(G_0, G_t, \theta)$ based on Eq. 6;
 Update denoiser s_θ via gradients $\nabla_\theta \mathcal{L}_t$.

generation [29], we adopt this conditional independence assumption to make score composition tractable, while recognizing that handling correlated conditions remains an important direction for future research.

This decomposition leads to the definition of our CoG score [29]:

$$s_\theta^{\text{CoG}}(G_t, \mathcal{C}, t) = s_\theta(G_t, \emptyset, t) + \sum_{m=1}^M w_m \left(s_\theta(G_t, c_m, t) - s_\theta(G_t, \emptyset, t) \right). \quad (9)$$

This CoG strategy modulates the contribution of each single property-specific score $s_\theta(G_t, c_m, t)$ via a corresponding guidance scale w_m . Such a formulation provides fine-grained control, enabling selective emphasis on specific subsets of properties during sampling.

To enable CoG, we train a the denoiser s_θ following the procedure described in Algorithm 1. During training, each condition c_m is picked with a fixed probability, s_θ is enabled to jointly learn the conditional score functions $s_\theta(G_t, c_m, t)$ for each $c_m \in \mathcal{C}$ and the unconditional one $s_\theta(G_t, \emptyset, t)$ in a unified way. At inference time (Algorithm 2), these scores are combined via the CoG strategy to guide generation toward arbitrary subsets of target properties.

3.3. Probability Calibration with Concrete Scores

After obtaining the guided score, we compute the transition probabilities $p_{s|t}^\theta(G_s|G_t; \theta)$ according to Eq. (5). Although guidance improves condition alignment, it may also compromise sample fidelity.

Algorithm 2: Sampling from Score-based Graph Diffusion Model with CoG.

Input: Trained denoiser s_θ , base distribution p_{base} , transition matrices Q^X, Q^E , noise schedule $\bar{\sigma}$, specified timesteps $0 = t_0 < \dots < t_T = 1$, specified properties $\mathcal{C}' = \{c_{m_1}, \dots, c_{m_L}\}, 1 \leq m_1 < \dots < m_L \leq M$.

Output: Sampled graph G

Sample $G_T \sim p_{\text{base}}, k \leftarrow T$;

while $k > 0$ **do**

 Compute unconditional score $s_\theta(G_t, \emptyset, t_k)$;

for each $1 \leq l \leq L$ **do**

 Compute conditional score: $s_\theta(G_t, c_{m_l}, t_k)$;

 Compute CoG scores $s_\theta^{\text{CoG}}(G_t, \mathcal{C}', t_k)$ based on Eq. 9;

 Construct transition densities $p_{t_{k-1}|t_k}^X(x_{t_{k-1}}^i | x_{t_k}^i; \theta)$ and $p_{t_{k-1}|t_k}^E(e_{t_{k-1}}^{ij} | e_{t_k}^{ij}; \theta)$ by substituting s_θ by s_θ^{CoG} based on Eq. 4;

 Apply PC to transition densities $p_{t_{k-1}|t_k}^X(x_{t_{k-1}}^i | x_{t_k}^i; \theta)$ and $p_{t_{k-1}|t_k}^E(e_{t_{k-1}}^{ij} | e_{t_k}^{ij}; \theta)$ as described in Section 3.3; // Optional

for each $1 \leq i \leq n$ **do**

 Sample $x_{t_{k-1}}^i \sim p_{t_{k-1}|t_k}^X(\cdot | x_{t_k}^i; \theta)$;

for each $1 \leq i, j \leq n$ **do**

 Sample $e_{t_{k-1}}^{ij} \sim p_{t_{k-1}|t_k}^E(\cdot | e_{t_k}^{ij}; \theta)$;

 Construct $G_{t_{k-1}} \leftarrow ((x_{t_{k-1}}^i)_{i=1}^n, (e_{t_{k-1}}^{ij})_{i,j=1}^n)$;

 Update $k \leftarrow k - 1$;

return $G \leftarrow G_0$

In particular, high guidance scales can cause a train–test mismatch [37], where the guided score, i.e., s_θ^{CoG} , during sampling falls outside the ranges observed in training. In our work, we observe a similar phenomenon which degrades both the validity and controllability of generated molecules. To address this, we apply *dynamic thresholding* and *temperature scaling*, which jointly calibrate the probabilities.

Dynamic Thresholding. Let p_{raw} denote the raw guided probabilities computed with s_θ^{CoG} based on Eq. 4. We first clamp negative entries to zero and compute the lower and upper percentiles (e.g., $\alpha = 1\%$, $\beta = 99\%$) across the state dimension: $\ell = \text{Quantile}(p_{\text{raw}}, \alpha)$, $h = \max(\text{Quantile}(p_{\text{raw}}, \beta), \ell + \varepsilon)$, where ε is a small constant (e.g., 10^{-6}) to avoid division by zero. The probabilities are then normalized by min–max scaling:

$$p_{\text{clipped}} = \frac{[p_{\text{raw}} - \ell]_+}{h - \ell}, \quad [p]_+ \equiv \max(p, 0). \quad (10)$$

This procedure guarantees valid probabilities in $[0, 1]$, stabilizing sampling by preventing extreme values from dominating. Our dynamic thresholding serves as a discrete analogue to Imagen’s method [37]: rather than scaling continuous pixel values, we calibrate discrete transition probabilities by percentile-based clipping, ensuring well regularized probability ranges during sampling.

Temperature Scaling. Temperature scaling is a post-processing method used to improve probabilistic predictions in classification tasks [14, 25, 46]. Its impact on graph diffusion sampling remains unexplored. Here, we investigate whether temperature scaling can improve the validity and controllability of generated graphs by modulating the sharpness of the predicted distributions at each step of sampling. To this end, we further adjust the distribution via temperature τ :

$$p_{\text{scaled}}(i) = \frac{(p_{\text{clipped}}(i))^{1/\tau}}{\sum_j (p_{\text{clipped}}(j))^{1/\tau}} \text{ for each outcome } i. \quad (11)$$

Lower τ (i.e., $0 < \tau < 1$) sharpens the distribution and favors high-probability states, while higher τ (i.e., $\tau > 1$) flattens it and promotes diversity.

Probability Calibration combines percentile thresholding and temperature scaling to calibrate guided probability, enhancing both validity and controllability in molecular graph generation. In practice, it involves three key parameters: α , β , and τ . Based on our experience, τ is the parameter most worth tuning, while α and β can be assigned reasonable values to ensure stability (e.g., $\alpha = 1\%$, $\beta = 99\%$).

4. Experiments

To evaluate the effectiveness of extending score matching to discrete graph diffusion models, as well as the score-based capacities it enables, namely, composable guidance (CoG) and probability calibration (PC), we conducted comprehensive quantitative experiments to answer the following research questions: **RQ1**: Does CSGD outperform related discrete graph diffusion models? **RQ2**: Can concrete scores improve the quality and controllability of samples relative to the mean prediction approach? **RQ3**: How beneficial are CoG and PC for generating valid and controllable samples in multi-conditional generation? **RQ4**: Can CoG support flexible sampling under varying numbers and types of molecular property conditions?

4.1. Experimental Setup

Datasets. Following the experimental setup in GraphDiT [28], we evaluate multi-conditional molecular generation using two types of datasets: (1) For materials design, we use a Polymers dataset [47], which includes four numerical conditions related to synthesizability—Synthetic Accessibility Score (SAS) [10] and Synthetic Complexity Score (SCS) [6]—as well as gas permeability properties (O_2P , N_2P , and CO_2P). (2) For drug design, we evaluate on three class-balanced dataset—BACE, BBBP, and HIV—from MoleculeNet [43]. Each dataset provides a categorical condition specific to its task (e.g., blood–brain barrier permeability for BBBP, β -secretase 1 inhibition for BACE, and HIV replication inhibition for HIV), together with the same numerical synthesizability conditions (SAS and SCS) used in the Polymers dataset.

Metrics. To systematically evaluate model performance, we use over three classes of metrics covering generation quality, distribution Learning, and controllability. First, we assess **Validity**, defined as the proportion of valid molecules among generated samples. Second, we evaluate the model’s ability to learn the target distribution using three metrics: **Diversity** (measured by Tanimoto similarity [3] among generated molecules), **Similarity** (fragment-based similarity to the reference set), and **FCD** [34] (Fréchet ChemNet Distance) between generated and reference distributions. Third, we

Table 1: Results on the Polymers dataset including four numerical conditions. The best-performing methods for each metric are highlighted in bold, and the second-best are underlined.

Model	Validity \uparrow	Distribution Learning				Controllability		
		Diversity \uparrow	Similarity \uparrow	FCD \downarrow	Synth. \downarrow	O ₂ P. \downarrow	N ₂ P. \downarrow	CO ₂ P. \downarrow
DiGress	<u>99.13</u>	<u>0.9099</u>	0.2724	22.7237	2.9842	1.7163	2.0630	1.6738
DiGress v2	98.12	0.9105	0.2771	21.7311	2.7507	1.7130	2.0632	1.6648
GDSS	92.05	0.7510	0.0000	34.2627	1.3701	1.0271	1.0820	1.0683
MOOD	98.66	0.8349	0.0227	39.3981	1.4019	1.4961	1.7603	1.4748
GraphDiT	82.45	0.8712	0.9600	<u>6.6443</u>	1.2973	0.7440	0.8857	0.7550
CSGD Absorb	95.07	0.8793	<u>0.9568</u>	6.8110	<u>1.2572</u>	<u>0.7311</u>	<u>0.8754</u>	<u>0.7466</u>
CSGD Uniform	99.38	0.8683	0.9541	6.4351	1.1905	0.6054	0.6993	0.6232

measure controllability: for numerical conditions, we report the **MAE** between the specified conditions and predicted properties of the generated molecules; for categorical conditions, we report **Accuracy**.

Baselines. We compare our method with recent diffusion-based models for multi-conditional molecular generation, including GDSS [20], DiGress [41], and their conditional variants MOOD [27] and DiGress v2, as well as GraphDiT [28], which represents the current state-of-the-art in this task. For MOOD and DiGress v2, trained multi-task property predictors with the same architecture are used to provide guidance. We note that GraphDiT adopts a graph-dependent forward diffusion process, which demonstrates superior performance within its full model pipeline [28]. This creates a noise-model mismatch relative to our independent tokenwise scheme. If anything, this discrepancy may favor GraphDiT, making our evaluation of CSGD conservative and thus fair under these conditions.

Implementation Details. Our implementation builds on the official open-source code of GraphDiT [28], leveraging its Graph Transformer and condition encoder to handle both numerical and categorical properties. We split each dataset into training, validation, and test sets with a 6:2:2 ratio. For evaluation, we generate 10,000 molecules conditioned on the properties of the reference set. Generation validity and distributional metrics are computed using the MOSES [33]. For controllability evaluation, we follow GraphDiT and adopt a random forest model trained on all task-related molecules as an Oracle [11]. The properties of samples are then compared with the specified conditions to calculate MAE/Accuracy for numerical/categorical property.

4.2. (RQ1) Overall Performance Comparison

We first compare the overall performance of CSGD with both CoG and PC against existing baselines across all the adopted datasets.

We present the results on the Polymers dataset in Table 1, where CSGD consistently achieves notable improvements over the most competing baseline GraphDiT in both validity and controllability. With a transition matrix leading to the *Uniform* p_{base} , CSGD attains an average relative improvement in MAE of +15.3% compared to the strongest baseline. While DiGress and its v2 variant generate diverse molecules, they struggle to satisfy multiple conditions simultaneously, leading to weaker controllability and lower FCD scores. In contrast, CSGD not only maintains strong distribution learning but also achieves the best FCD, confirming the effectiveness of CSGD.

Table 2: Comparisons with both numerical and categorical conditions evaluated by MAE and Accuracy, respectively. The best-performing methods for each metric are highlighted in bold, and the second-best are underlined.

Dataset	Model	Validity \uparrow	Distribution Learning			Controllability	
			Diversity \uparrow	Similarity \uparrow	FCD \downarrow	MAE \downarrow	Accuracy \uparrow
HIV	DiGress	43.77	<u>0.9194</u>	0.8562	13.0409	1.9216	0.5335
	DiGress v2	50.50	0.9193	0.8476	13.3997	1.5934	0.5331
	GDSS	69.26	0.7817	0.1032	45.3416	1.2515	0.4830
	MOOD	28.75	0.9280	0.1361	32.3523	2.3144	0.5106
	GraphDiT	69.06	0.8983	<u>0.9580</u>	6.0605	0.3825	0.9437
	SDGD Absorb	<u>76.30</u>	0.8973	0.9584	5.9495	0.2531	<u>0.9755</u>
	SDGD Uniform	83.36	0.8945	0.9519	<u>6.0499</u>	<u>0.3560</u>	0.9898
BBBP	DiGress	69.60	0.9098	0.6805	18.6921	2.3658	0.6536
	DiGress v2	68.92	<u>0.9107</u>	0.6336	19.4498	2.2694	0.6531
	GDSS	62.18	0.8415	0.2672	39.9440	1.3788	0.5037
	MOOD	80.08	0.9273	0.1715	34.2506	2.0284	0.4903
	GraphDiT	78.72	0.8891	0.9281	11.3367	<u>0.4492</u>	0.9089
	SDGD Absorb	<u>86.24</u>	0.8895	<u>0.9335</u>	<u>10.9960</u>	0.4354	<u>0.9398</u>
	SDGD Uniform	95.63	0.8807	0.9467	10.8411	1.0745	0.9831
BACE	DiGress	35.11	<u>0.8862</u>	0.6942	24.6560	2.0681	0.5061
	DiGress v2	35.46	0.8812	0.7027	25.3270	2.3365	0.5113
	GDSS	28.79	0.8756	0.2708	46.7539	1.6422	0.5036
	MOOD	99.47	0.8902	0.2587	44.2394	1.8853	0.5062
	GraphDiT	76.00	0.8256	0.8780	6.9663	<u>0.4171</u>	<u>0.9132</u>
	SDGD Absorb	77.20	0.8251	<u>0.8786</u>	6.1112	0.3963	0.8884
	SDGD Uniform	<u>96.92</u>	0.8133	0.8935	<u>6.7618</u>	0.8221	0.9250

Results on datasets with both numerical and categorical conditions (see Table 2) further confirm these findings. CSGD achieves the best validity and controllability, while maintaining competitive distribution learning, particularly in terms of FCD and similarity. These results demonstrate that CSGD can flexibly guide the generation of molecular graphs in diverse conditional settings, producing valid molecules with improved compliance to the specified properties.

4.3. Ablation Studies

To assess the contribution of each component, we conduct a detailed ablation study focusing on two aspects: score-based modeling in graph diffusion and two score manipulation techniques.

4.3.1. (RQ2) PERFORMANCE OF SCORE-BASED MODELING

Score-based modeling is evaluated against the current mean-prediction approach, GraphDiT, using the same guidance strategy. Due to space constraints, we report results on two datasets in Table 3, with the complete results across all four datasets provided in Appendix (see Table 6). For clarity, results on the Polymers dataset are reported as the average MAE of gas permeability across all gases, rather than per-gas MAE.

Table 3: Ablation (RQ2): Comparing CSGD (w/o PC, and with CFG rather than CoG) to GraphDiT with CFG, where numerical and categorical conditions are evaluated using MAE and Accuracy, respectively.

Dataset	Model	Validity \uparrow	Controllability		
			Synth. \downarrow	Gas Perm. \downarrow	Inhibition \uparrow
Polymers	GraphDiT	82.45	1.2973	0.9205	-
	CSGD Absorb	<u>90.15</u>	1.1129	0.8940	-
	CSGD Uniform	95.81	<u>1.2779</u>	<u>0.9179</u>	-
HIV	GraphDiT	69.06	0.3825	-	0.9437
	CSGD Absorb	<u>74.01</u>	0.3035	-	<u>0.9761</u>
	CSGD Uniform	81.30	<u>0.3650</u>	-	0.9898

The most notable improvement is in molecular validity, with CSGD achieving better performance under both *Absorb* and *Uniform* p_{base} . Improvements in controllability also remain competitive. Taken together, these findings indicate that score-based modeling substantially improves the validity and controllability of discrete graph diffusion in multi-conditional generation.

Table 4: Ablation (RQ3): Comparison of CoG and CFG in CSGD with and without PC. Numerical and categorical conditions are evaluated using MAE and Accuracy, respectively.

Dataset	Strategy	Probability Calibration	Validity \uparrow	Controllability		
				Synth. \downarrow	Gas Perm. \downarrow	Inhibition \uparrow
Polymers	CFG	\times	95.81	1.2779	0.9179	-
		\checkmark	99.51	1.1815	0.8088	-
	CoG	\times	98.84	1.1784	0.7968	-
		\checkmark	99.36	1.1905	0.7796	-
HIV	CFG	\times	81.30	0.3650	-	0.9898
		\checkmark	82.34	0.3418	-	0.9910
	CoG	\times	80.89	0.3855	-	0.9869
		\checkmark	83.36	0.3560	-	0.9898

4.3.2. (RQ3) EFFECTIVENESS OF COMPOSABLE GUIDANCE AND PROBABILITY CALIBRATION

As shown in Table 4, we evaluate the effectiveness of CoG on two datasets, with results on all four benchmarks provided in the Appendix (see Table 7). Under the same network architecture, hyperparameters, and guidance scale, CoG achieves performance comparable to CFG with a *Uniform* p_{base} . For instance, CSGD with CoG attains 98.84% validity while maintaining strong controllability. Across other datasets, CoG consistently matches CFG in performance while enabling flexible sampling of CSGD, underscoring its practicality for multi-conditional molecular generation.

We further assess the effect of PC under both CFG and CoG. Across all datasets and guidance strategies, incorporating PC consistently enhances validity and controllability. Despite its simplicity, PC proves to be a practical and effective tool, serving as a general, plug-and-play component to improve diverse score-manipulation techniques in molecular graph generation.

Table 5: (RQ4): Comparison of CSGD performance when sampling with different subsets of properties specified. * Total guidance weight of each subset is kept the same. Synth.: Synthesizability; O₂, N₂, CO₂: Gas Permeability.

Model	Property Subsets*	Validity↑	Controllability			
			Synth.↓	O ₂ P.↓	N ₂ P.↓	CO ₂ P.↓
GraphDiT	{Synth., O ₂ , N ₂ , CO ₂ }	82.45	1.2973	0.7440	0.8857	0.7550
	{Synth., O ₂ , N ₂ , CO ₂ }	99.38	1.1905	0.6054	0.6993	0.6232
CSGD	{Synth.}	99.78	0.9179	-	-	-
	{O ₂ , N ₂ , CO ₂ }	99.38	-	0.6001	0.6927	0.6133
	{Synth., O ₂ }	99.50	1.1894	0.6099	-	-

4.4. (RQ4) Flexibility

To evaluate the flexibility of CSGD, we conduct experiments on the Polymers dataset, which contains two types of four properties and is well-suited for this analysis. Using the same trained models, we assess CSGD under different property subsets, including the full set, single-type subsets (e.g., Synthesizability alone or only Gas Permeability properties), and mixed-type subsets (e.g., Synthesizability combined with a single Gas Permeability property).

As shown in Table 5, CoG enables flexible sampling by conditioning generation on arbitrary subsets of properties. When conditioning solely on Synthesizability or the Gas Permeability properties (O₂, N₂, CO₂), the model achieves the best controllability for the targeted property while maintaining high validity, suggesting that focusing on a single property allows more precise control. For mixed subsets (e.g., Synthesizability combined with O₂), the model effectively balances multiple objectives, achieving strong validity and good controllability on the selected properties. Overall, these results demonstrate that CoG supports flexible and practical multi-conditional generation, enabling molecular design to be tailored to diverse application needs.

4.5. Conclusion and Future Directions

In this work, inspired by the flexibility of score-based modeling in continuous-state diffusion, we introduce concrete scores for discrete graph diffusion. By bridging the gap between discrete molecular structures and score-based modeling, concrete scores open the door to applying a wide range of score-based techniques to discrete graph domains. To demonstrate their flexibility and effectiveness, we propose two novel strategies and validate them on the challenging task of multi-conditional molecular generation. We demonstrate that CSGD achieves strong performance and exhibits high flexibility on several multi-conditional molecular generation benchmarks.

Recent progress in discrete flow matching—notably Discrete Flow Matching (DFM) for general discrete data [12] and its graph-specialized variant DeFoG [35]—offers an alternative generative paradigm that disentangles training and sampling for increased efficiency. In contrast, our

method operates within a score-based diffusion framework, enabling principled score composability and flexible multi-conditional control; exploring hybrid approaches that combine composable score guidance with the sampling efficiency of discrete flow matching is an exciting direction for future work. Moreover, we hope to extend our framework to a wider range of graph generation domains such as citation and social networks, providing a unified foundation for controllable graph generative modeling.

References

- [1] Donghoon Ahn, Hyoungwon Cho, Jaewon Min, Wooseok Jang, Jungwoo Kim, SeonHwa Kim, Hyun Hee Park, Kyong Hwan Jin, and Seungryong Kim. Self-rectifying diffusion sampling with perturbed-attention guidance. In *European Conference on Computer Vision (ECCV)*, pages 1–17. Springer, 2024.
- [2] Jacob Austin, Daniel D Johnson, Jonathan Ho, Daniel Tarlow, and Rianne Van Den Berg. Structured denoising diffusion models in discrete state-spaces. *Advances in Neural Information Processing Systems (NeurIPS)*, 34:17981–17993, 2021.
- [3] Dávid Bajusz, Anita Rácz, and Károly Héberger. Why is tanimoto index an appropriate choice for fingerprint-based similarity calculations? *Journal of Cheminformatics*, 7:1–13, 2015.
- [4] Camille Bilodeau, Wengong Jin, Tommi Jaakkola, Regina Barzilay, and Klavs F Jensen. Generative models for molecular discovery: Recent advances and challenges. *Wiley Interdisciplinary Reviews: Computational Molecular Science*, 12(5):e1608, 2022.
- [5] Andrew Campbell, Joe Benton, Valentin De Bortoli, Thomas Rainforth, George Deligiannidis, and Arnaud Doucet. A continuous time framework for discrete denoising models. *Advances in Neural Information Processing Systems (NeurIPS)*, 35:28266–28279, 2022.
- [6] Connor W Coley, Luke Rogers, William H Green, and Klavs F Jensen. Scscore: synthetic complexity learned from a reaction corpus. *Journal of Chemical Information and Modeling*, 58(2):252–261, 2018.
- [7] Prafulla Dhariwal and Alexander Nichol. Diffusion models beat gans on image synthesis. *Advances in Neural Information Processing Systems (NeurIPS)*, 34:8780–8794, 2021.
- [8] Yuanqi Du, Arian R Jamasb, Jeff Guo, Tianfan Fu, Charles Harris, Yingheng Wang, Chenru Duan, Pietro Liò, Philippe Schwaller, and Tom L Blundell. Machine learning-aided generative molecular design. *Nature Machine Intelligence*, 6(6):589–604, 2024.
- [9] Bradley Efron. Tweedie’s formula and selection bias. *Journal of the American Statistical Association*, 106(496):1602–1614, 2011.
- [10] Peter Ertl and Ansgar Schuffenhauer. Estimation of synthetic accessibility score of drug-like molecules based on molecular complexity and fragment contributions. *Journal of Cheminformatics*, 1(1):8, 2009.
- [11] Wenhao Gao, Tianfan Fu, Jimeng Sun, and Connor Coley. Sample efficiency matters: a benchmark for practical molecular optimization. *Advances in Neural Information Processing Systems (NeurIPS)*, 35:21342–21357, 2022.

- [12] Itai Gat, Tal Remez, Neta Shaul, Felix Kreuk, Ricky T. Q. Chen, Gabriel Synnaeve, Yossi Adi, and Yaron Lipman. Discrete flow matching. In *The Thirty-eighth Annual Conference on Neural Information Processing Systems*, 2024.
- [13] Niklas WA Gebauer, Michael Gastegger, Stefaan SP Hessmann, Klaus-Robert Müller, and Kristof T Schütt. Inverse design of 3d molecular structures with conditional generative neural networks. *Nature Communications*, 13(1):973, 2022.
- [14] Chuan Guo, Geoff Pleiss, Yu Sun, and Kilian Q Weinberger. On calibration of modern neural networks. In *International Conference on Machine Learning (ICML)*, pages 1321–1330. PMLR, 2017.
- [15] Kaiming He, Xiangyu Zhang, Shaoqing Ren, and Jian Sun. Deep residual learning for image recognition. In *The IEEE/CVF Conference on Computer Vision and Pattern Recognition (CVPR)*, pages 770–778, 2016.
- [16] Jonathan Ho and Tim Salimans. Classifier-free diffusion guidance. In *NeurIPS 2021 Workshop on Deep Generative Models and Downstream Applications (NeurIPS Workshop)*, 2021.
- [17] Jonathan Ho, Ajay Jain, and Pieter Abbeel. Denoising diffusion probabilistic models. *Advances in Neural Information Processing Systems (NeurIPS)*, 33:6840–6851, 2020.
- [18] Vincent Tao Hu, David W Zhang, Yuki M Asano, Gertjan J Burghouts, and Cees GM Snoek. Self-guided diffusion models. In *The IEEE/CVF Conference on Computer Vision and Pattern Recognition (CVPR)*, pages 18413–18422, 2023.
- [19] Xun Huang and Serge Belongie. Arbitrary style transfer in real-time with adaptive instance normalization. In *International Conference on Computer Vision (ICCV)*, pages 1501–1510, 2017.
- [20] Jaehyeong Jo, Seul Lee, and Sung Ju Hwang. Score-based generative modeling of graphs via the system of stochastic differential equations. In *International Conference on Machine Learning (ICML)*, pages 10362–10383, 2022.
- [21] Tim Kaiser, Nikolas Adaloglou, and Markus Kollmann. The unreasonable effectiveness of guidance for diffusion models. *arXiv preprint arXiv:2411.10257*, 2024.
- [22] Tero Karras, Miika Aittala, Tuomas Kynkäänniemi, Jaakko Lehtinen, Timo Aila, and Samuli Laine. Guiding a diffusion model with a bad version of itself. *Advances in Neural Information Processing Systems (NeurIPS)*, 37:52996–53021, 2024.
- [23] Frank P Kelly. Reversibility and stochastic networks. *PF Kelly—New York: Willy*, 1981.
- [24] Diederik P. Kingma and Jimmy Ba. Adam: A method for stochastic optimization. In *International Conference on Learning Representations (ICLR)*, 2015.
- [25] Meelis Kull, Miquel Perello Nieto, Markus Kängsepp, Telmo Silva Filho, Hao Song, and Peter Flach. Beyond temperature scaling: Obtaining well-calibrated multi-class probabilities with dirichlet calibration. *Advances in Neural Information Processing Systems (NeurIPS)*, 32, 2019.

- [26] Tuomas Kynkäänniemi, Miika Aittala, Tero Karras, Samuli Laine, Timo Aila, and Jaakko Lehtinen. Applying guidance in a limited interval improves sample and distribution quality in diffusion models. *Advances in Neural Information Processing Systems (NeurIPS)*, 37:122458–122483, 2024.
- [27] Seul Lee, Jaehyeong Jo, and Sung Ju Hwang. Exploring chemical space with score-based out-of-distribution generation. In *International Conference on Machine Learning (ICML)*, pages 18872–18892. PMLR, 2023.
- [28] Gang Liu, Jiaxin Xu, Tengfei Luo, and Meng Jiang. Graph diffusion transformers for multi-conditional molecular generation. *Advances in Neural Information Processing Systems (NeurIPS)*, 37:8065–8092, 2024.
- [29] Nan Liu, Shuang Li, Yilun Du, Antonio Torralba, and Joshua B Tenenbaum. Compositional visual generation with composable diffusion models. In *European Conference on Computer Vision (ECCV)*, pages 423–439. Springer, 2022.
- [30] Aaron Lou, Chenlin Meng, and Stefano Ermon. Discrete diffusion modeling by estimating the ratios of the data distribution. In *International Conference on Machine Learning (ICML)*, pages 32819–32848, 2024.
- [31] Chenlin Meng, Kristy Choi, Jiaming Song, and Stefano Ermon. Concrete score matching: Generalized score matching for discrete data. *Advances in Neural Information Processing Systems (NeurIPS)*, 35:34532–34545, 2022.
- [32] Chenhao Niu, Yang Song, Jiaming Song, Shengjia Zhao, Aditya Grover, and Stefano Ermon. Permutation invariant graph generation via score-based generative modeling. In *International Conference on Artificial Intelligence and Statistics (AISTATS)*, pages 4474–4484. PMLR, 2020.
- [33] Daniil Polykovskiy, Alexander Zhebrak, Benjamin Sanchez-Lengeling, Sergey Golovanov, Oktai Tatanov, Stanislav Belyaev, Rauf Kurbanov, Aleksey Artamonov, Vladimir Aladinskiy, Mark Veselov, et al. Molecular sets (moses): a benchmarking platform for molecular generation models. *Frontiers in Pharmacology*, 11:565644, 2020.
- [34] Kristina Preuer, Philipp Renz, Thomas Unterthiner, Sepp Hochreiter, and Gunter Klambauer. Fréchet chemnet distance: a metric for generative models for molecules in drug discovery. *Journal of Chemical Information and Modeling*, 58(9):1736–1741, 2018.
- [35] Yiming Qin, Manuel Madeira, Dorina Thanou, and Pascal Frossard. Defog: Discrete flow matching for graph generation. In *International Conference on Machine Learning (ICML)*, 2025.
- [36] Seyedmorteza Sadat, Manuel Kansy, Otmar Hilliges, and Romann M Weber. No training, no problem: Rethinking classifier-free guidance for diffusion models. In *International Conference on Learning Representations (ICLR)*, 2025.

- [37] Chitwan Saharia, William Chan, Saurabh Saxena, Lala Li, Jay Whang, Emily L Denton, Kamyar Ghasemipour, Raphael Gontijo Lopes, Burcu Karagol Ayan, Tim Salimans, et al. Photorealistic text-to-image diffusion models with deep language understanding. *Advances in Neural Information Processing Systems (NeurIPS)*, 35:36479–36494, 2022.
- [38] Antoine Siraudin, Fragkiskos D Malliaros, and Christopher Morris. Cometh: A continuous-time discrete-state graph diffusion model. *arXiv preprint arXiv:2406.06449*, 2024.
- [39] Yang Song, Jascha Sohl-Dickstein, Diederik P Kingma, Abhishek Kumar, Stefano Ermon, and Ben Poole. Score-based generative modeling through stochastic differential equations. In *International Conference on Learning Representations (ICLR)*, 2021.
- [40] Haoran Sun, Lijun Yu, Bo Dai, Dale Schuurmans, and Hanjun Dai. Score-based continuous-time discrete diffusion models. In *International Conference on Learning Representations (ICLR)*, 2023.
- [41] Clement Vignac, Igor Krawczuk, Antoine Siraudin, Bohan Wang, Volkan Cevher, and Pascal Frossard. Digress: Discrete denoising diffusion for graph generation. In *International Conference on Learning Representations (ICLR)*, 2023.
- [42] Zixu Wang, Yangyang Chen, Pengsen Ma, Zhou Yu, Jianmin Wang, Yuansheng Liu, Xiucui Ye, Tetsuya Sakurai, and Xiangxiang Zeng. Image-based generation for molecule design with sketchmol. *Nature Machine Intelligence*, 7(2):244–255, 2025.
- [43] Zhenqin Wu, Bharath Ramsundar, Evan N Feinberg, Joseph Gomes, Caleb Geniesse, Aneesh S Pappu, Karl Leswing, and Vijay Pande. Moleculenet: a benchmark for molecular machine learning. *Chemical science*, 9(2):513–530, 2018.
- [44] Minkai Xu, Lantao Yu, Yang Song, Chence Shi, Stefano Ermon, and Jian Tang. Geodiff: A geometric diffusion model for molecular conformation generation. In *International Conference on Learning Representations (ICLR)*, 2022.
- [45] Zhe Xu, Ruizhong Qiu, Yuzhong Chen, Huiyuan Chen, Xiran Fan, Menghai Pan, Zhichen Zeng, Mahashweta Das, and Hanghang Tong. Discrete-state continuous-time diffusion for graph generation. *Advances in Neural Information Processing Systems (NeurIPS)*, 37:79704–79740, 2024.
- [46] Hao Xuan, Bokai Yang, and Xingyu Li. Exploring the impact of temperature scaling in softmax for classification and adversarial robustness. *arXiv preprint arXiv:2502.20604*, 2025.
- [47] Yuri Yampolskii. Polymeric gas separation membranes. *Macromolecules*, 45(8):3298–3311, 2012.
- [48] Candi Zheng and Yuan Lan. Characteristic guidance: Non-linear correction for diffusion model at large guidance scale. In *International Conference on Machine Learning (ICML)*, pages 61386–61412, 2024.

5. Full Ablation Results

Tables 6 and 7 provide the complete ablation results across all four datasets, complementing the condensed versions shown in the main text. Table 6 compares CSGD (without PC) with CFG against GraphDiT using the same guidance strategy, reporting validity and controllability metrics (Avg. MAE for Polymers, Property Accuracy for HIV, BBBP, and BACE). Table 7 further examines the effects of Composable Guidance (CoG) and Probability Calibration (PC) under both CFG and CoG strategies, highlighting all metrics improved by PC. These full tables allow a comprehensive view of our method’s performance and ablation effects across all datasets.

Table 6: Ablation (RQ2): Comparing CSGD (w/o PC, and with CFG rather than CoG) to GraphDiT with CFG, where numerical and categorical conditions are evaluated using MAE and Accuracy, respectively.

Dataset	Model	Validity \uparrow	Controllability		
			Synth. \downarrow	Gas Perm. \downarrow	Accuracy \uparrow
Polymers	GraphDiT	82.45	1.2973	0.9205	-
	CSGD Absorb	<u>90.15</u>	1.1129	0.8940	-
	CSGD Uniform	95.81	<u>1.2779</u>	<u>0.9179</u>	-
HIV	GraphDiT	69.06	0.3825	-	0.9437
	CSGD Absorb	<u>74.01</u>	0.3035	-	<u>0.9761</u>
	CSGD Uniform	81.30	<u>0.3650</u>	-	0.9898
BBBP	GraphDiT	78.72	0.4492	-	0.9089
	CSGD Absorb	<u>86.58</u>	<u>0.4625</u>	-	<u>0.9449</u>
	CSGD Uniform	88.02	1.1669	-	0.9725
BACE	GraphDiT	76.00	<u>0.4171</u>	-	<u>0.9132</u>
	CSGD Absorb	<u>78.08</u>	0.3904	-	0.8998
	CSGD Uniform	92.23	0.8683	-	0.9290

6. Supplementary Details about Experiments

All data and code used in this work are publicly available at our GitHub repository: <https://github.com/anjie-qiao/CSGD>.

All experiments are trained and evaluated on a single NVIDIA A800-80GB-PCIE GPU. We provide default configuration files and fixed random seeds to ensure that all reported results can be fully reproduced. Training CSGD on each of these four datasets can be completed within 24 hours. The final checkpoint is used for evaluation.

6.0.1. DATASETS

We evaluate CSGD on four datasets: one for materials design (Polymers) and three for drug design (HIV, BACE, and BBBP). The Polymers dataset contains four numerical conditions. The first condition, synthesizability, combines two scores—Synthetic Accessibility Score (SAS) and Synthetic Complexity Score (SCS)—concatenated as a two-dimensional vector, e.g., [6.1, 2.29]. The remain-

Table 7: Ablation (RQ3): Comparison of CoG and CFG in CSGD with and without PC. Metrics improved by PC are highlighted in bold. Numerical and categorical conditions are evaluated using MAE and Accuracy, respectively.

Dataset	Transition Matrix	Strategy	Probability Calibration	Validity \uparrow	Controllability		
					Synth. \downarrow	Gas Perm. \downarrow	Accuracy \uparrow
Polymers	Absorb	CFG	\times	90.15	1.1129	0.8940	-
			\checkmark	90.89	1.1264	0.8791	-
	Uniform	CoG	\times	94.89	1.2506	0.9066	-
			\checkmark	95.07	1.2572	0.9026	-
	Uniform	CFG	\times	95.81	1.2779	0.9179	-
			\checkmark	99.51	1.1815	0.8088	-
Uniform	CoG	\times	98.84	1.1784	0.7968	-	
		\checkmark	99.36	1.1905	0.7796	-	
HIV	Absorb	CFG	\times	74.01	0.3035	-	0.9761
			\checkmark	75.95	0.2840	-	0.9770
	Uniform	CoG	\times	75.74	0.2548	-	0.9745
			\checkmark	76.30	0.2531	-	0.9755
	Uniform	CFG	\times	81.30	0.3650	-	0.9898
			\checkmark	82.34	0.3418	-	0.9910
Uniform	CoG	\times	80.89	0.3855	-	0.9869	
		\checkmark	83.36	0.3560	-	0.9898	
BBBP	Absorb	CFG	\times	86.58	0.4625	-	0.9449
			\checkmark	86.15	0.4494	-	0.9458
	Uniform	CoG	\times	85.12	0.4375	-	0.9449
			\checkmark	86.24	0.4354	-	0.9398
	Uniform	CFG	\times	88.02	1.1669	-	0.9725
			\checkmark	94.42	1.0707	-	0.9793
Uniform	CoG	\times	86.09	1.1801	-	0.9705	
		\checkmark	95.63	1.0745	-	0.9831	
BACE	Absorb	CFG	\times	78.08	0.3904	-	0.8998
			\checkmark	78.18	0.3891	-	0.9073
	Uniform	CoG	\times	77.20	0.4033	-	0.8874
			\checkmark	77.42	0.3964	-	0.8884
	Uniform	CFG	\times	92.23	0.8683	-	0.9290
			\checkmark	95.74	0.8326	-	0.9395
Uniform	CoG	\times	95.81	0.8547	-	0.9183	
		\checkmark	96.92	0.8221	-	0.9250	

ing three conditions correspond to gas permeability (O_2 , N_2 , and CO_2), each represented by a single numerical value, e.g., 2.8, 1.5, and 15.4.

For the drug design datasets, each sample includes both a numerical and a categorical condition. The numerical condition is the same two-dimensional synthesizability vector used in Polymers. The categorical condition is a binary label indicating a task-specific property, e.g., for HIV, whether

a molecule inhibits HIV replication (1 indicates inhibition, 0 otherwise). All three drug design datasets are class-balanced.

Following GraphDiT, We randomly split each dataset into training, validation, and test sets with a 6:2:2 ratio. A fixed random seed is used to ensure that the splits are reproducible and do not affect result replication.

6.0.2. DIFFUSION DETAILS

Our score-based diffusion model is built on the official SEDD implementation. Following SEDD, we use a log-linear noise schedule: $\bar{\sigma}(t) = -\log(1 - (1 - \epsilon t))$, where $\epsilon = 10^{-5}$ is a small constant to ensure numerical stability as $t \rightarrow 1$.

We adopt the architecture and hyperparameters from GraphDiT, with only minor changes such as adjusting epochs and learning rate. Specifically, all models are trained with a batch size of 1200, a learning rate of 3×10^{-4} , and gradient clipping with a maximum norm of 1. A linear warm-up is applied for the first 1500 iterations. The number of diffusion steps is set to 1000.

6.0.3. CONDITION ENCODERS

To enable multi-conditional molecular generation, we employ separate encoders for categorical and numerical properties, following GraphDiT.

Categorical Encoder. Categorical conditions (e.g., task-specific labels such as HIV inhibition) are embedded using a *Categorical Encoder*. Each category $c \in \{0, \dots, K-1\}$ is mapped to a learnable vector $\mathbf{e}_c \in \mathbb{R}^{d_h}$:

$$\mathbf{e}_c = \text{Embed}(c'), \quad c' = \begin{cases} K, & \text{with probability } p_{\text{drop}}, \\ c, & \text{otherwise,} \end{cases} \quad (12)$$

where $\text{Embed}(\cdot)$ is a learnable table of size $(K + 1) \times d_h$. Dropout of individual labels allows simultaneous learning of conditional and unconditional estimates.

Cluster Encoder. Numerical conditions $c \in \mathbb{R}^{d_{\text{in}}}$ are embedded using a *Cluster Encoder*. The embedding is given by

$$\mathbf{e}_c = \begin{cases} \mathbf{e}_{\emptyset}, & \text{with probability } p_{\text{drop}}, \\ \text{MLP}(c), & \text{otherwise,} \end{cases} \quad (13)$$

where $\text{MLP}(\cdot)$ is a two-layer network with an intermediate Softmax, and \mathbf{e}_{\emptyset} is a learnable null embedding shared across dropped conditions.

These two encoders together allow diffusion model to flexibly incorporate arbitrary combinations of categorical and numerical conditions during both training and sampling.

6.0.4. THE DENOISING NETWORK.

Our denoising network is built upon the GraphDiT architecture. Given a noisy molecular graph at timestep t , the node and edge features are first concatenated and projected into a hidden space \mathbf{H} via a linear layer. These representations are then processed by a stack of Graph Transformer [28] (GT)

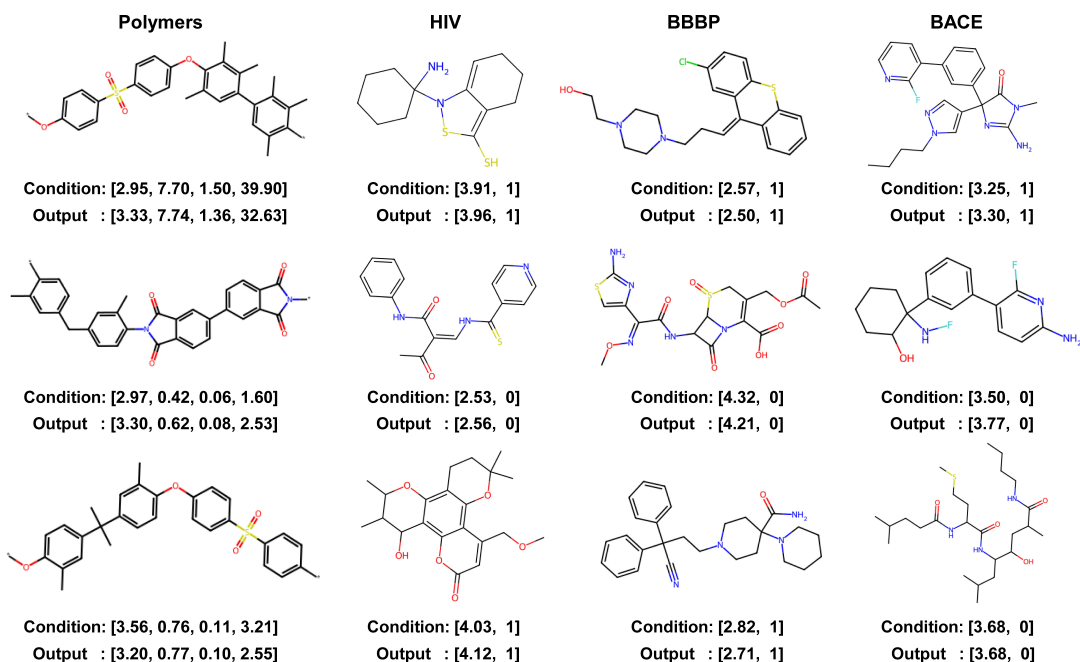


Figure 3: Generated molecular graphs across the four datasets. The **Condition** refer to the input properties, while the **Output** correspond to the properties of the generated molecules. For the Polymers dataset, the four properties are Synthesizability, and Gas Permeabilities of O₂, N₂, and CO₂. For the HIV, BBBP, and BACE datasets, the two properties are Synthesizability and a task-specific property (e.g., HIV inhibition).

layers equipped with adaptive layer normalization [19] (AdaLN), where the normalization parameters are modulated by the combined condition and timestep embeddings $e_y = e_c + e_t$. Formally, the hidden states \mathbf{H} are updated as

$$\mathbf{H} = \text{GT}(\mathbf{H}, e_y),$$

integrating conditional information. The final hidden states are passed through an MLP with AdaLN:

$$\mathbf{H}_{\text{output}} = \text{AdaLN}(\text{MLP}(\mathbf{H}), e_y),$$

and then split into atom and bond components, $\mathbf{H}_{\text{output}}^X$ and $\mathbf{H}_{\text{output}}^E$, which correspond to the predicted node and edge log-concrete scores s_{θ}^X and s_{θ}^E . This design allows the network to jointly reason about atom types and bond structures while flexibly incorporating both categorical and numerical conditions.

6.1. Visualization

We visualize samples generated by CSGD across the four datasets, as shown in Figure 6.0.3. These examples demonstrate that CSGD is able to generate molecules that closely adhere to the specified input multi-conditions.